12th International Symposium on Turbulence and Shear Flow Phenomena (TSFP12)
Osaka, Japan (Online), July 19-22, 2022

LARGE EDDY SIMULATIONS OF A TURBULENT BOUNDARY LAYER WITH UNSTEADY PRESSURE GRADIENTS

Francesco Ambrogi
Dept. of Mechanical and Materials Eng.
Queen's University
Kingston, ON Canada
f.ambrogi@queensu.ca

Ugo Piomelli
Dept. of Mechanical and Materials Eng.
Queen's University
Kingston, ON Canada
ugo@queensu.ca

David E. Rival
Dept. of Mechanical and Materials Eng.
Queen's University
Kingston, ON Canada
d.e.rival@queensu.ca

ABSTRACT

We use large-eddy simulations to investigate a spatially developing turbulent boundary layer with a space- and time-dependent pressure gradient. The flow oscillates between times in which a favorable pressure gradient is followed by an adverse one, a zero-pressure gradient, and a period in which the adverse pressure gradient is followed by a favorable one. The alternating favorable and adverse pressure gradient causes the flow to separate periodically and reattach from the wall. Several cases have been investigated for a range of reduced frequencies, spanning the range between a very rapid flutter-like motions to a slower quasi-steady flapping. Time- and phase-averaged fields are analyzed, and comparison is made with steady cases with fixed pressure gradients.

INTRODUCTION

Almost all turbulent boundary-layer flows of practical relevance are subject to pressure gradients, usually introduced by geometric changes. The pressure gradient may be favorable (FPG) or adverse (APG) depending on whether the pressure decreases or increases along the flow direction. Both conditions are very common in engineering and physical systems such as airfoils or turbine blades, and in geophysical applications.

If the APG is strong enough, the boundary layer may separate from the wall. Flow separation can significantly affect the efficiency of fluidic devices. A comprehensive review on the physics of flow separation can be found in Simpson (1989). A strong FPG, on the other hand, may lead to a relaminarization of the turbulent boundary layer (TBL) caused by the predominance of pressure forces over the turbulent Reynolds stresses (Narasimha & Sreenivasan, 1973). More complete reviews of the flow in FPG and APG boundary layers (both experiments and numerical simulations) can be found in papers by Fernholz & Warnack (1998) and Wu & Piomelli (2018) for APG TBL, and Bourassa & Thomas (2009); Piomelli & Yuan (2013) for the FPG case.

Most studies of APG and FPG boundary layers consider pressure-gradients that are constant or vary only spatially. However, in many cases (e.g., helicopter blades, turbine blades, pitching airfoils etc.) the pressure gradient varies both spatially and temporally. In fish locomotion, for instance, unsteady pressure gradients are the norm: fish propel themselves by waving their tail, and (especially during maneuvers) the changing body curvature generates unsteadiness in the pressure distribution along the body, and pressure gradients that are space and time dependent (Domenici *et al.*, 2004).

While the steady flow in APG and FPG TBLs has been studied extensively (see the papers referenced above, and many others) fewer investigations of the unsteady case can be found (Schatzman & Thomas, 2017). In the present paper we consider an unsteady spatially developing FPG/APG turbulent boundary layer, which was simulated using wall-resolved large-eddy simulations (LES). By oscillating the freestream velocity periodically in time, we were able generate a flow field that can either separate or tend towards re-laminarization, depending on the phase of the cycle. Various frequencies of oscillations are considered. The Reynolds number is moderate, but large enough to result in a fully developed equilibrium TBL if no pressure gradient is applied. In addition, we also performed steady calculations with time-independent pressure gradients at selected phases, for comparison with the dynamic cases.

Although much effort has been invested to shed light into the complexity of separated flows, many questions still remain unanswered: (1) How is the reduced frequency affecting the separation cycle of a flat-plate TBL? (2) What are the underlying physical characteristics behind the phenomenon of dynamic hysteresis and their effects on the flow behavior? In the present work, results will be presented to answer these questions.

NUMERICAL METHODOLOGY

In the present work, simulations are performed using the Large Eddy Simulation (LES) technique. In LES, the incompressible Navier Stokes equations are solved for filtered quan-

tities (here indicated with an overline):

$$\frac{\partial \overline{u}_i}{\partial x_i} = 0; \quad \frac{\partial \overline{u}_i}{\partial t} + \frac{\partial}{\partial x_j}\left(\overline{u}_i \overline{u}_j\right) = -\frac{\partial \overline{p}}{\partial x_i} + \nu \nabla^2 \overline{u}_i - \frac{\partial \tau_{ij}}{\partial x_j} \quad (1)$$

where, (x,y,z) are the streamwise, wall-normal, and spanwise directions, and $\tau_{ij} = \overline{u_i u_j} - \overline{u}_i \overline{u}_j$ is the sub-filter scale stress tensor. In the present study τ_{ij} is modelled using the Vreman eddy-viscosity model (Vreman, 2004). We use a well-validated finite-difference code that has previously been applied to similar cases (Keating *et al.*, 2004; Yuan & Piomelli, 2015; Wu & Piomelli, 2018). The dimensions of the computational domain are $L_x = 600\delta_o^*$, $L_y = 64\delta_o^*$, and $L_z = 55\delta_o^*$. δ_o^* is the boundary layer displacement thickness at the inflow plane. The Reynolds number based on δ_o^* and the freestream velocity at the inflow (which is constant in time) is $Re_{\delta_o^*} = 1{,}000$. The grid uses $N_x \times N_y \times N_z = 1536 \times 192 \times 256$ points; a grid-convergence study was performed to verify that this resolution is adequate. In wall units (defined using the wall shear velocity u_τ at the inflow plane) we have $\Delta x^+ = 18.7$, $\Delta y^+_{\min} = 0.7$, and $\Delta z^+ = 10$. A periodic boundary condition is used in the spanwise direction, a convective boundary condition at the outflow plane, and a velocity obtained from a parallel auxiliary simulation is used at the inflow.

The pressure gradient is generated by imposing a vertical velocity $V_\infty(x,t)$ at the free-stream that changes both in space and time, $V_\infty(x,t) = V_o(x)\sin(2\pi t/T)$, where T is the oscillation period, and V_o a streamwise distribution of wall-normal velocity, which was chosen to match the case studied by Na & Moin (1998). The streamwise freestream velocity is obtained by imposing a zero vorticity condition (Lund *et al.*, 1998; Na & Moin, 1998; Wu & Piomelli, 2018).

The non dimensional parameter that characterizes the unsteadiness is the reduced frequency $k = \pi f L_{PG}/U_o$, where $f = 2\pi/T$ is the imposed frequency, L_{PG} is a characteristic length (we use the length over which the Pressure Gradient varies), and U_o is the free-stream velocity at the inflow plane. We performed numerical simulations for $k = 0.2,\ 1$ and 10. Leishman (2006) found that a reduced frequency $k > 0.05$ was the threshold beyond which the boundary layer was clearly unsteady, and many experimental studies have been carried out for a wide range of reduced frequency $0.1 < k < 82$ (Karlsson, 1959; Brunton & Rowley, 2009). In our case the definition of the length-scale is not unique, and we chose the length of the region where the pressure-gradient is significant as the one that most closely resembles the chord length of an airfoil. Because of this arbitrariness, a one-to-one comparison with the studies in the literature is difficult; however, we obtained trends that are in agreement with the results in the literature, as will be shown momentarily.

The oscillation period was divided into 20 equally spaced phases, and phase averaging (here indicated with $\langle\cdot\rangle$) has been carried out for every quantity. As shown in Figure 1, if ϕ is the phase angle, $\phi = 0^o$ and 180^o degrees correspond to a zero-pressure gradient (ZPG) case, whereas at 270^o an APG is followed by an FPG, and at 90^o the FPG precedes the APG. We also carried out numerical simulations with a steady pressure gradient corresponding to that imposed at $\phi = 0^\circ,\ 54^\circ,\ 90^\circ,\ 270^\circ$, and 306°.

RESULTS

FLOW EVOLUTION

The first important result is the effect of the reduced frequency k on flow separation. Figure 2 shows contours of phase-averaged steamwise velocity $\langle u\rangle$ for the extreme phase $\Phi = 270^\circ$. We can observe that flow separation (on average) occurs in each of the unsteady cases though the size of the separation region greatly changes as the frequency k decreases. For the high and medium frequency cases ($k = 10$ and $k = 1$) the separation region does not have the time to grow as thick as in the corresponding steady case (Figure 2 d), however it is very interesting to note that the length of the separation region for the $k = 10$ case is comparable with the corresponding steady case, but the length of the separation region for the $k = 1$ case is significantly lower. This behavior will be explained in the following section. As the frequency k is reduced to 0.2, a quasi-steady state is approached, and the dimensions of the separation bubble (both height and length) match very well the steady calculation. Table 1 summarizes the dimensions of the separation bubbles; here X_S and X_R are the averaged separation and reattachment locations in the streamwise direction.

Figure 4 shows the behavior of the phase-avergaed streamwise velocity $\langle u\rangle$ for the medium frequency case $k = 1$. As discussed above, as the frequency decreases, the thickness

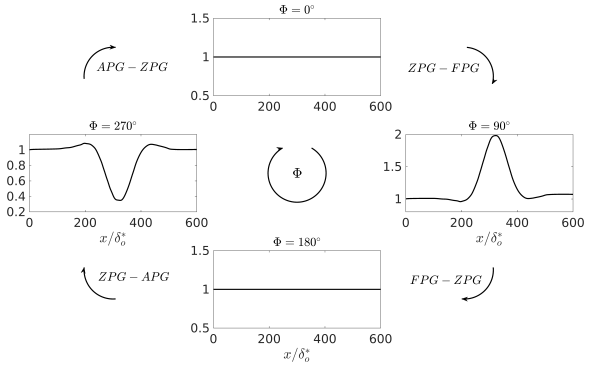

Figure 1. Freestream velocity at four phases in the cycle. Black arrows denoting the direction of increasing phase angle Φ.

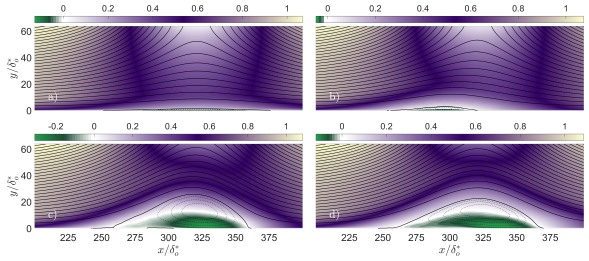

Figure 2. Contours of phase-averaged streamwise velocity $\langle u\rangle$ for the phase $\Phi = 270^\circ$. (a) $k = 10$; (b) $k = 1$; (c) $k = 0.2$; (d) Steady calculation.

Case	X_S/δ_o^*	H/δ_o^*	L/δ_o^*	X_R/δ_o^*
$k = 10$	251	1.4	124	375
$k = 1$	253	3.2	67	320
$k = 0.2$	240	25	120	360
Steady	247	23	122	369

Table 1. Dimensions of the four separation bubbles for the unsteady and steady cases at $\Phi = 270^\circ$.

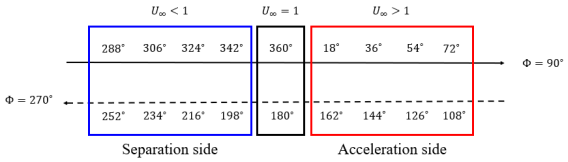

Figure 3. Schematic representation of all matching phases in one complete cycle. Following the black solid line from the extreme phase $\Phi = 270^\circ$ the cycle reaches the opposite extreme $\Phi = 90^\circ$ and goes back following the black dashed line towards completion of the cycle.

of the separation bubble increases but the length of the separation region is significantly reduced (see phase $\Phi = 270^\circ$ Figure 4). Moreover, the separation region is highly unstable, and the slow-moving fluid, generated by the flow reversal, is advected downstream and periodically washed out of the domain (Simpson, 1989). This peculiar flow dynamics has only been observed for the $k = 1$ case, which indicates that there is a limiting frequency k beyond which the recirculation vortex is shed. This behavior is consistent with experimental observations of a pulsating flow over a backward-facing step. A critical frequency $F^* = 0.07$, defined using the step height h and the mean velocity $\overline{U}$, was found, after which the shedding occurred (Mullin *et al.*, 1980; Simpson, 1989).

Finally Figure 5 shows phase-averaged streamwise velocity $\langle u \rangle$ profiles for 4 phases in the cycle at 3 different streamwise locations in the domain: $x/\delta_o^* = 270, 300, 450$ corresponding to locations upstream, at the center, and downstream of the pressure gradient region. At $\Phi = 90^\circ$, in the acceleration side of the cycle where $U_\infty > 1$, the dynamic cases match very well the steady calculations (black dots in Figure 5), with the best agreement being the lowest frequency $k = 0.2$. At $\Phi = 270^\circ$ on the other hand, in the separation side of the cycle where $U_\infty < 1$, great differences arise. First, we observe the difference between the dynamic cases, which is due to the different size and development of the separation bubbles. Second, even though the case $k = 0.2$ is approaching a quasi-steady-state, displaying a good match with the steady calculation, it is characterized by a stronger backflow in the center of the separation region indicating the persistence of transient effects.

The most interesting case however, can be visualized by comparing $\Phi = 0^\circ$ and $\Phi = 180^\circ$ in Figure 5. At these two phases, the boundary layer is experiencing the same pressure gradient, specifically zero in both cases. The main difference between the two phases is that in the first case ($\Phi = 0^\circ$) the flow is going towards the acceleration side of the cycle, in the second case, the flow is coming from the acceleration side and going towards separation. Very evident from Figure 5 is that while $k = 10$ (very high) and $k = 0.2$ (very low) frequencies match reasonably well the steady calculation, $k = 1$ case displays discrepancies in the velocity profiles. This suggests that the advection of the stalled fluid region downstream of the separation bubble is generating significant hysteresis effects.

HYSTERESIS EFFECTS

Dynamic hysteresis is observed when a physical quantity assumes two different values at corresponding phases in a periodic cycle. As shown by the schematic representation in Figure 3, dividing the cycle in 20 equally spaced phases results in a total of 9 matching phases in which the boundary layer is experiencing the same pressure gradient twice in one cycle. The phases are divided into three groups: the first (blue square in Figure 3) includes phases in the separation side of the cycle, where the APG precedes the FPG, and the freestream velocity $U_\infty < 1$. The second (black square in Figure 3) includes the two phases characterized by a ZPG. The third group (red square in Figure 3) includes the phases in the acceleration side of the cycle, where the FPG precedes the APG, and $U_\infty > 1$.

In order to visualize the hysteresis effects we can observe the behavior of the velocity profile at a selected streamwise location for every phase in the cycle. If there were no hysteresis effects, the velocity profile for matching phases should be the same. Figure 6 shows results for the high frequency case $k = 10$ in the streamwise location $x/\delta_o^* = 300$. Due to the high frequency (large k), the convective time-scale of the flow (L_{PG}/U_o) is dominant over the unsteady imposed one ($1/\pi f$). The velocity at the matching phases is in good agreement, except for a very thin layer close to the wall. Hysteresis effects are therefore concentrated very close to the wall, where viscosity causes a small lag in the response to the freestream acceleration/deceleration. We can also observe that, at phase $\Phi = 198^\circ$, corresponding to the instant when the freestream forcing (V_∞ velocity profile) turns from blowing-suction to suction-blowing, the flow separates until it reaches the extreme phase $\Phi = 270^\circ$. At this frequency the flow is synchronized with the freestream forcing everywhere except for a very small near-wall region where friction generates dynamic hysteresis.

For the $k = 1$ case, Figure 7, at the same streamwise location, hysteresis effects are moving away from the wall towards the center of the separated shear-layer. The convective time-scale of the flow and the unsteady imposed one are now comparable, resulting in a significant lag in response of the near-wall fluid to the freestream forcing. In fact, coming back from the acceleration side (close to $\Phi = 90^\circ$) and moving towards separation, although the freestream velocity U_∞ is decelerating, the velocity is significantly higher compared to the corresponding matching phase, and the flow does not separate until $\Phi = 234^\circ$ when the magnitude of V_∞ reaches 70% of its maximum value.

As the frequency is further decreased ($k = 0.2$), at the same streamwise location, the unsteady imposed time-scale is now dominant over the convective one, and given the very long oscillation period T, the flow has time to adapt to the freestream perturbations. Although the flow is moving towards a quasi-steady state as shown in Figure 5, hysteresis effects still play a significant role in the domain. However, a crucial difference from the other two cases is that, at this frequency, dynamic hysteresis effects are confined to the separation side of the cycle whereas all the matching phases in the acceleration side show very good agreement.

CONCLUDING REMARKS

Large-eddy simulations of a spatially-developing turbulent boundary layer with space- and time-dependent pressure gradients have been carried out. The unsteadiness was imposed by oscillating the freestream vertical velocity V_∞ periodically. The maximum adverse pressure gradient was strong enough to generate a large-scale turbulent separation bubble in the domain. Simulations have been performed for a range of reduced frequency $k = 10, 1, 0.2$, and results have been compared with steady calculations at the same instantaneous pressure gradient.

Two main questions have been driving our research: 1) How is the reduced frequency k affecting the separation cycle of a flat-plate TBL? (2) What are the underlying physical characteristics behind the phenomenon of dynamic hysteresis and their effects on the flow behavior?

The reduced frequency k plays a crucial role in the flow configuration and the characteristics of the transient flow separation. If k is large enough ($k = 10$) the separation bubble (formed at the center of the domain) does not have time to grow as thick as in the corresponding steady case, but the length of the separation region is comparable. For the medium frequency case, on the other hand, we observed a growth of the separation bubble in the wall-normal direction, but the length of the separation region significantly decreased compared to the steady case. At this frequency the separation region is highly unstable and is periodically advected downstream, and washed out of the domain (Mullin *et al.*, 1980; Simpson, 1989). Although the lowest frequency case $k = 0.2$ shows a trend towards a quasi-steady state, transient effects persist in the separation region.

Dynamic hysteresis was observed in all unsteady cases. Specifically, when the convective time-scale of the flow dominates over the imposed unsteady one ($k = 10$), hysteresis effects are confined to the near-wall region, and the flow behavior is synchronized everywhere with the freestream forcing. As the frequency decreases, hysteresis effects move away from the wall towards the center of the separated shear-layer. When $k = 1$, the two time-scales are comparable and the response of the near-wall fluid lags significantly the freestream forcing. In the lowest frequency case, the unsteady time scale is now dominant over the convective one, and the flow has time to adapt to the freestream forcing, however hysteresis effects are still observed in the separation side of the cycle.

REFERENCES

Bourassa, C. & Thomas, F. O. 2009 An experimental investigation of a highly accelerated turbulent boundary layer. *J. Fluid Mech.* **634**, 359–404.

Brunton, S. & Rowley, C. 2009 Modeling the unsteady aerodynamic forces on small-scale wings. AIAA Paper 2009-1127.

Domenici, P., Standen, E. M. & Levine, R. P. 2004 Escape manoeuvres in the spiny dogfish (squalus acanthias). *J. Exp. Biol.* **207** (13), 2339–2349.

Fernholz, H. H. & Warnack, D. 1998 The effects of a favourable pressure gradient and of the reynolds number on an incompressible axisymmetric turbulent boundary layer. part 1. the turbulent boundary layer. *J. Fluid Mech.* **359**, 329–356.

Karlsson, S. K. F. 1959 An unsteady turbulent boundary layer. *J. Fluid Mech.* **5** (4), 622–636.

Keating, A., Piomelli, U., Bremhorst, K. & Nešić, S. 2004 Large-eddy simulation of heat transfer downstream of a backward-facing step. *J. Turb.* **5** (1), 020.

Leishman, G. J. 2006 *Principles of helicopter aerodynamics*. Cambridge U. P.

Lund, T. S., Wu, X. & Squires, K. D. 1998 Generation of inflow data for spatially-developing boundary layer simulations. *J. Comput. Phys.* **140**, 233–258.

Mullin, T., Greated, C. A. & Grant, I. 1980 Pulsating flow over a step. *Phys. Fluids* **23** (4), 669–674.

Na, Y. & Moin, P. 1998 Direct numerical simulation of a separated turbulent boundary layer. *J. Fluid Mech.* **374**, 379–405.

Narasimha, R. & Sreenivasan, K. R. 1973 Relaminarization in highly accelerated turbulent boundary layers. *J. Fluid Mech.* **61** (3), 417–447.

Piomelli, U. & Yuan, J. 2013 Numerical simulations of spatially developing, accelerating boundary layers. *Phys. Fluids* **25**, 101304–1—21.

Schatzman, D. M. & Thomas, F. O. 2017 An experimental investigation of an unsteady adverse pressure gradient turbulent boundary layer: embedded shear layer scaling. *J. Fluid Mech.* **815**, 592.

Simpson, R. L. 1989 Turbulent boundary-layer separation. *Ann. Rev. Fluid Mech.* **21** (1), 205–232.

Vreman, A. W. 2004 An eddy-viscosity subgrid-scale model for turbulent shear flow: Algebraic theory and applications. *Phys. Fluids* **16** (10), 3670–3681.

Wu, W. & Piomelli, U. 2018 Effects of surface roughness on a separating turbulent boundary layer. *J. Fluid Mech.* **841**, 552–580.

Yuan, J. & Piomelli, U. 2015 Numerical simulation of a spatially developing accelerating boundary layer over roughness. *J. Fluid Mech.* **780**, 192–214.

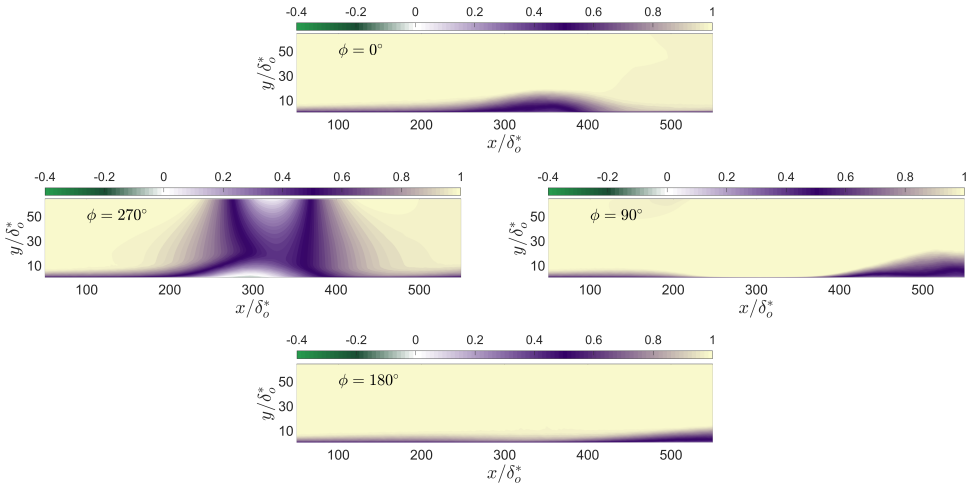

Figure 4. Contours of phase-averaged streamwise velocity $\langle u \rangle$ for $k = 1$. Only the main four phases of the cycle are shown: $\Phi = 0°$, $\Phi = 90°$, $\Phi = 180°$, and $\Phi = 270°$.

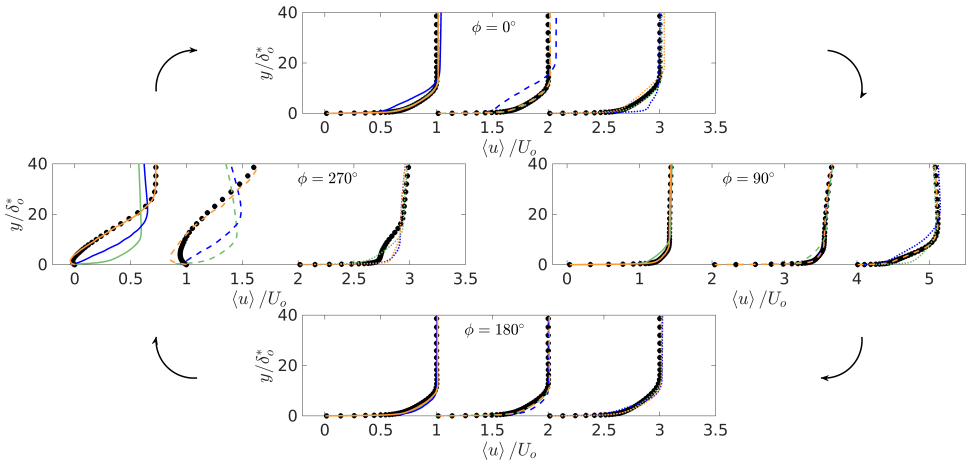

Figure 5. Streamwise phase-averaged $\langle u \rangle$ velocity profile for four phases in the cycle for the different reduced frequencies k (colours) and streamwise locations (line styles). Comparison is made with steady calculations (symbols) at the same streamwise locations. Each profile is shifted by one unit for clarity. Solid line: $x/\delta_o^* = 270$ dashed line: $x/\delta_o^* = 300$; dotted line: $x/\delta_o^* = 450$. • Steady case; — $k = 10$; — $k = 1$; — $k = 0.2$.

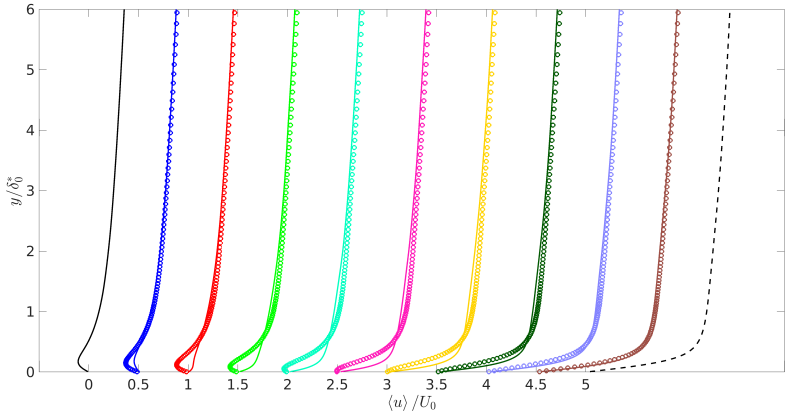

Figure 6. Phase-averaged streamwise velocity for the $k = 10$ case at the streamwise location $x/\delta_o^* = 300$. All key phases are displayed. Black solid and dashed lines represent the extreme phases $\Phi = 270°$ and $\Phi = 90°$ respectively, corresponding to APG-FPG and FPG-APG. Colours represent the intermediate phases in the cycle. The solid line represent the phases between 270° and 90° (APG-ZPG and ZPG FPG phases), and symbols represent the matching phases from 90° to 270° (FPG-ZPG and ZPG-APG phases). — $\Phi = 270°$; - - $\Phi = 90°$; — ○ $\Phi = 288°,\ 252°$; — ○ $\Phi = 306°,\ 234°$; — ○ $\Phi = 324°,\ 216°$; — ○ $\Phi = 342°,\ 198°$; — ○ $\Phi = 0°,\ 180°$; — ○ $\Phi = 18°,\ 162°$; — ○ $\Phi = 36°,\ 144°$; — ○ $\Phi = 54°,\ 126°$; — ○ $\Phi = 72°,\ 108°$.

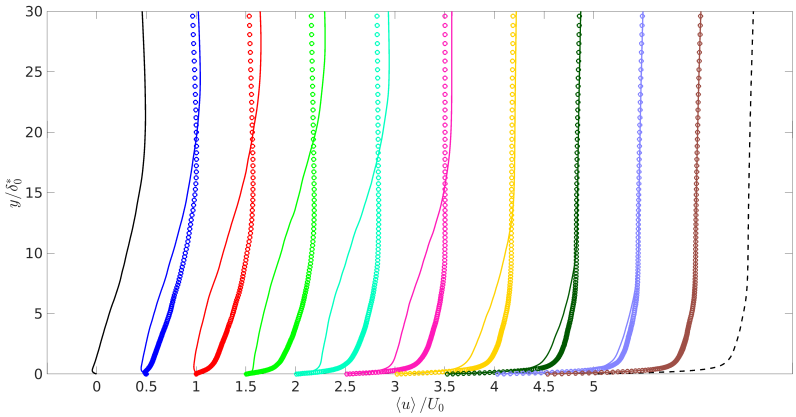

Figure 7. Phase-averaged streamwise velocity for the $k = 1$ case at the streamwise location $x/\delta_o^* = 300$. All key phases are displayed. The same notation as in Figure 6 is used.

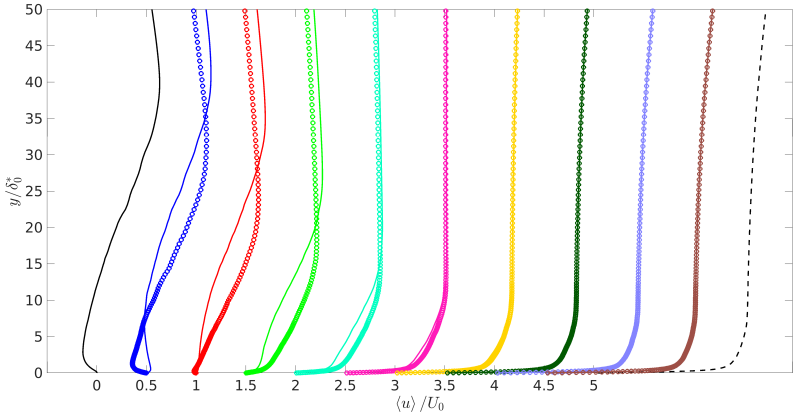

Figure 8. Phase-averaged streamwise velocity for the $k = 0.2$ case at the streamwise location $x/\delta_o^* = 300$. All key phases are displayed. The same notation as in Figure 6 is used.